JAST, Vol. 14, No. 2, pp. 66-79
© Iranian Aerospace Society, Summer-Fall 2021

JAST Journal of Aerospace Science and Technology

Scientific-Research Article

Nonlinear Thermal Buckling of FG Cylindrical Panels using Dynamic Relaxation Method and Incremental Loading Approach

M.E. Golmakani [1*], M. Moravej[2], M. Sadeghian[3]

1-2-3. Department of Mechanical Engineering, Mashhad Branch, Islamic Azad University, Mashhad, Iran

*Email: m.e.golmakani@mshdiau.ac.ir

In this paper, the nonlinear thermal buckling of moderately thick and functionally graded cylindrical panels is analyzed based on the first-order shear deformation theory (FSDT) and large deflection von Kármán equations. The highly coupled nonlinear governing equations are solved using a combination of dynamic relaxation approach with the finite-difference discretization method in various boundary conditions. The material properties of the constituent components of the FG shell are considered to vary continuously along the thickness direction based on simple power-law and Mori-Tanaka distribution methods, separately. The critical thermal buckling load is considered based on the thermal load-displacement curve derived by solving the incremental form of nonlinear equilibrium equations. In order to consider the accuracy of the present results, a comparison study has been carried out. The effects of the boundary conditions, rule of mixture, grading index, radius-to-thickness ratio, length-to-radius ratio, and panel angle are studied on the thermal buckling loads. It is observed from the results that in high values of radius-to-thickness ratios, there is no difference between the values of critical buckling temperature differences for linear and nonlinear distributions.

Keywords: *Nonlinear; Thermal Buckling; Functionally graded panel; Dynamic relaxation method.*

Introduction

Flat and curved panels are important subjects of engineering applications among the different structural components. These sorts of panels can be subjected to thermal loading which the increase of temperature may lead to compressive stresses in the panels under imposed specific boundary conditions; therefore, it may cause thermal buckling failures of the panels. Recently Carbon nanotube-reinforced (CNT) [1-3], reinforced functionally graded (FG) plates [4-6] have been investigated. Functionally graded materials (FGMs) have received a lot of attention. In the case of thermal analysis, FGMs can withstand high temperatures keeping structural integrity at the same time. In other words, FGMs properties show a smooth variation from one surface to another which omit interface problems and decrease stress concentration [7,8]. Despite the significant importance of the buckling of cylindrical panels, few published papers are available [9-11]. Norouzi and Alibeigloo [12] studied thermo-viscoelastic behavior of cylindrical FGM panel subjected to thermal and/or mechanical load using 3D elasticity theory. In their paper, they utilized the Fourier series expansion and state-space approach. Seifi et al. [13] investigated the buckling load of cracked panels subjected to compressive and tensile axial loads as force per unit length. They noticed radius, thickness, width, and length of the panels have

1. Assistant Professor (Corresponding Author)
2. M.Sc. graduate
2. PhD Candidate

Received: 12 October 2020
Accepted: 27 April 2021

little impact on the buckling load of the cracked panels. Using the Rayleigh–Ritz approach and Kirchhoff–Love's hypotheses, Panahandeh et al. [14] studied the buckling of cylindrical panels on tensionless elastic foundations subjected to axial compression. They noticed that the impact of the foundation on buckling of the panel is significantly dependent on width-to-thickness ratio, foundation modulus, aspect ratio, and central angle. Magnucki [15] investigated nonlinear symmetrically mechanical buckling of the cylindrical panel. Using the principle of stationary potential energy, he derived differential equations of equilibrium. Golmakani et al. [16] studied nonlinear buckling of moderately thick functionally graded (FG) cylindrical panels under axial compression for different boundary conditions based on the First-order shear deformation theory (FSDT) via dynamic relaxation (DR) method. They observed that with the increase of grading index, the influence of radius-to-thickness ratio on the buckling load reduces. Zhang et al. [17] investigated thermal buckling of FG plates using a local Kriging meshless method. Duc and Tung [18] used classical shell theory to analyze the nonlinear behavior of FGM cylindrical panels subjected to uniform lateral pressure with and without temperature impacts in the simply supported condition. Authors of papers [19-21] studied mechanical and thermal buckling and post-buckling of conical and cylindrical FG shell panels based on FSDT via the element-free KP- Ritz approach. Dung and Hoa [22] analyzed nonlinear buckling and post-buckling of axially compressed FG cylindrical panels based on the classical shell theory. The Refs. [23,24] studied thermal buckling of the functionally graded cylindrical shell.

Despite the important contributions to the analysis of buckling behavior of cylindrical panels, so far, the nonlinear thermal buckling of FG cylindrical panels in various boundary conditions has not been studied based on FSDT, yet. Therefore, the present article analyzes the thermal buckling of FG cylindrical panels with clamped and simply supported boundary conditions according to FSDT and large deflection von Kármán equations. The DR technique combined with the finite difference (FD) discretization approach is employed to solve the governing equations. However, up to now, the thermal buckling behavior of FG cylindrical panels has not been considered using the DR technique, yet. In this paper, the critical thermal buckling load is considered based on the thermal load-displacement curve derived by solving the incremental form of nonlinear equilibrium equations. In order to estimate the elastic properties of actual FGM's accurately, the Mori-Tanaka model is utilized. Moreover, the results of this theory are also compared with the power-law distribution (simple rule of mixture) which showed a notable difference. Also, linear and nonlinear temperature distributions are assumed along the thickness direction. In order to consider the accuracy of the present results, a comparison study has been carried out. Finally, numerical results for critical temperature difference are obtained in diverse boundary conditions, two different rules of mixture, grading indices, radius -to- thickness, and length-to-radius ratios for linear and nonlinear types of thermal distributions.

Geometry and Material Properties

Fig. 1 shows an FG cylindrical panel with radius R, thickness h, and length L in the cylindrical coordinate system (x, θ, z). The FG panel is assumed as a mixture of ceramic and metal. Also, properties of it change continuously and smoothly through the thickness of the panel.

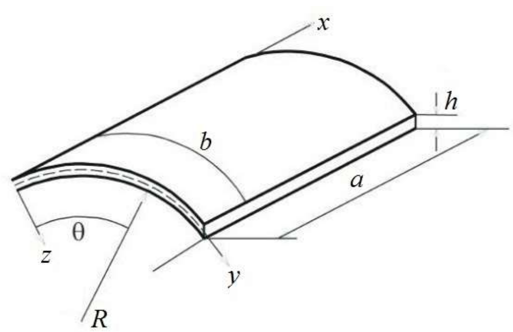

Fig 1. The geometry and coordinate system of the FG cylindrical panel

Although the power-law distribution of the volume fraction model is mainly considered to predict the elastic behaviors of FGMs, in some case studies, the Mori-Tanaka scheme [25] was utilized to validate the results with the power-law distribution theory. From this model, the material properties P (which is the effective values of Young's modulus and the Poisson's ratio) along the thickness of the FG panel can be written as:

$$P(z) = P_c V_c + P_m V_m \quad (1)$$

where the subscripts c and m express the ceramic and the metallic constituents, respectively. Also, based on the power-law distribution, the volume fractions of the ceramic V_c and the metal V_m are as follows:

$$V_c = \left(\frac{2z + h}{2h}\right)^k \tag{2}$$

$$V_m = 1 - V_c \tag{3}$$

In the above equation, z is the thickness in the domain of $-h/2 \le z \le h/2$ and k is the grading index that denotes the material change trend through the thickness of the panel. The effective shear modulus G, and the effective bulk modulus B, and thermal expansion coefficient α, of the FGM considering the Mori-Tanaka homogenization approach are assumed as:

$$\frac{B - B_c}{B_m - B_c} = \frac{V_m}{1 + (1 - V_m)\frac{3(B_m - B_c)}{3B_c + 4G_c}} \tag{4}$$

$$\frac{G - G_c}{G_m - G_c} = \frac{V_m}{1 + (1 - V_m)\frac{G_m - G_c}{G_c + f_c}} \tag{5}$$

$$\frac{K - K_m}{K_c - K_m} = \frac{V_c}{1 + (1 - V_c)\frac{(K_c - K_m)}{3K_m}} \tag{6}$$

$$\frac{\propto - \propto_m}{\propto_c - \propto_m} = \frac{\left(\frac{1}{B} - \frac{1}{B_m}\right)}{\left(\frac{1}{B_c} - \frac{1}{B_m}\right)} \tag{7}$$

where,

$$f_c = \frac{G_c(9B_c + 8G_c)}{6(B_c + 2G_c)} \tag{8}$$

Based on this procedure, the Young's modulus E and the Poison's Ratio ϑ can be obtained by:

$$E = \frac{9BG}{3B + G} \tag{9}$$

$$\vartheta = \frac{3B - 2G}{2(3B + G)} \tag{10}$$

Thermal Load Distribution

In this paper, the temperature variation is considered to occur only in the thickness direction. For the mentioned one-dimensional temperature field, it is considered that the outer ceramic surface is exposed to higher temperatures compared to the inner metal surface. In this case, the temperature distribution along the thickness can be defined by the following one-dimensional Fourier equation of heat conduction as:

$$\frac{d}{dz}\left(k(z)\frac{dT(z)}{dz}\right) = 0 \tag{11}$$

Linear Temperature Distribution

According to the linear temperature distribution, the thermal load distribution along the thickness direction is considered as follows [25]:

$$T(z) = T_m + (T_c - T_m)\left(z + \frac{h}{2}\right) \tag{12}$$

where $T = T_c$ at $z = h/2$ and $T = T_m$ at $z = -h/2$.

Nonlinear Temperature Distribution

The nonlinear thermal distribution $T(z)$ can be obtained by solving Eq. (11) as follows [26]:

$$T(z) = T_m + (T_c - T_m)\int_{-h/2}^{z}\frac{dz}{K(z)}\Bigg/\int_{-h/2}^{h/2}\frac{dz}{K(z)} \tag{13}$$

The integrations of the above equation are obtained numerically by discretizing the panel along the thickness direction. It is notable that in Ref. [24] for obtaining the thermal buckling load of FG cylindrical panel, the linear temperature variation was assumed along the thickness direction.

Governing Equations

The displacement field based on the FSDT in the cylindrical coordinate system (x, θ, z) is as follows:

$$\begin{aligned} U(x,\theta,z) &= u(x,\theta) + z\varphi_x(x,\theta) \\ V(x,\theta,z) &= v(x,\theta) + z\varphi_\theta(x,\theta) \\ W(x,\theta,z) &= w(x,\theta) \end{aligned} \tag{14}$$

where U , V, and W are the displacements corresponding to the coordinate system and are functions of the spatial coordinates; $u(x,\theta)$, $v(x,\theta)$, and $w(x,\theta)$ are the middle surface displacements and $\varphi_x(x,\theta)$, $\varphi_\theta(x,\theta)$ describe the rotations about the θ and x axes, respectively. As stated, to obtain the buckling load via the DR technique, the equilibrium equations should be obtained in the incremental form. So, all of the following governing equations are derived in the incremental form of variables. According to the incremental nonlinear von Kármán strain-displacement relations, the strain components compatible with the displacement field of Eq. (14) are as follow [16]:

$$\delta\varepsilon_{XX} = \frac{\partial\delta u}{\partial X} + \frac{1}{2}\left(\frac{\partial\delta w}{\partial X}\right)^2 + \frac{\partial w}{\partial X}\frac{\partial\delta w}{\partial X} + z\frac{\partial\delta\varphi_X}{\partial X} \tag{15}$$

$$\delta\varepsilon_{\theta\theta} = \frac{1}{R}\frac{\partial\delta v}{\partial\theta} + \frac{\delta w}{R} + \frac{1}{R^2}\frac{\partial w}{\partial\theta}\frac{\partial\delta w}{\partial\theta} + \frac{1}{2R^2}\left(\frac{\partial\delta w}{\partial\theta}\right)^2 + \frac{z}{R}\frac{\partial\delta\varphi_\theta}{\partial\theta}$$

$$\delta\gamma_{X\theta} = \frac{1}{R}\frac{\partial\delta u}{\partial\theta} + \frac{\partial\delta v}{\partial X} + \frac{1}{R}\frac{\partial\delta w}{\partial X}\frac{\partial w}{\partial\theta} + \frac{1}{R}\frac{\partial w}{\partial X}\frac{\partial\delta w}{\partial\theta} + \frac{1}{R}\frac{\partial\delta w}{\partial X}\frac{\partial\delta w}{\partial\theta} + Z\left(\frac{\partial\delta\varphi_\theta}{\partial X} + \frac{1}{R}\frac{\partial\delta\varphi_X}{\partial\theta}\right)$$

$$\delta\gamma_{XZ} = \delta\varphi_X(x,\theta) + \frac{\partial\delta w}{\partial X}$$

$$\delta\gamma_{\theta Z} = \delta\varphi_\theta(x,\theta) + \frac{1}{R}\frac{\partial\delta w}{\partial\theta}$$

Utilizing the Hooke's law, the incremental constitutive thermoelastic relations can be expressed by [16, 24]:

$$\begin{aligned}
\delta\sigma_X &= \frac{E(Z)}{1-\vartheta^2}[\delta\varepsilon_{XX} + \vartheta\delta\varepsilon_{\theta\theta}] - \frac{E(Z)\alpha(Z)T(Z)}{1-\vartheta}\\
\delta\sigma_\theta &= \frac{E(Z)}{1-\vartheta^2}[\delta\varepsilon_{\theta\theta} + \vartheta\delta\varepsilon_{XX}] - \frac{E(Z)\alpha(Z)T(Z)}{1-\vartheta}\\
\delta\tau_{X\theta} &= \frac{E(Z)}{2(1+\vartheta)}[\delta\gamma_{X\theta}]\\
\delta\tau_{XZ} &= \frac{E(Z)}{2(1+\vartheta)}[\delta\gamma_{XZ}]\\
\delta\tau_{\theta Z} &= \frac{E(Z)}{2(1+\vartheta)}[\delta\gamma_{\theta Z}]
\end{aligned} \tag{16}$$

The stress and moment resultants ($N_r, N_\theta, Q_r, M_r, M_\theta$) can be obtained utilizing the relevant integration through the thickness [16, 24]:

$$\begin{aligned}
(\delta N_i, \delta M_i) &= \int_{-h/2}^{h/2} \delta\sigma_i\,(1,z)dz \qquad i = x,\theta,x\theta\\
\delta Q_i &= \int_{-h/2}^{h/2} \delta\sigma_{iz}\,dz \qquad i = x,\theta\\
(\delta N_i^T, \delta M_i^T) &= \int_{-h/2}^{h/2} \frac{E(Z)\alpha(Z)T(Z)}{1-\vartheta}(1,z)dz \qquad i = x,\theta
\end{aligned} \tag{17}$$

By substituting Eqs. (15) and (16) into Eq. (17), the incremental form of the constitutive relations in terms of displacement field can be obtained as [16]:

$$\begin{aligned}
\delta N_X &= A_{11}\left[\frac{\partial\delta u}{\partial X} + \frac{1}{2}\left(\frac{\partial\delta w}{\partial X}\right)^2 + \frac{\partial w}{\partial X}\frac{\partial\delta w}{\partial X}\right] + A_{12}\left[\frac{1}{R}\frac{\partial\delta v}{\partial\theta} + \frac{\delta w}{R} + \frac{1}{R^2}\frac{\partial w}{\partial\theta}\frac{\partial\delta w}{\partial\theta} + \frac{1}{2R^2}\left(\frac{\partial\delta w}{\partial\theta}\right)^2\right] + B_{11}\left[\frac{\partial\delta\varphi_X}{\partial x}\right] + B_{12}\left[\frac{1}{R}\frac{\partial\delta\varphi_\theta}{\partial\theta}\right] - \delta N_x^T\\
\delta N_\theta &= A_{12}\left[\frac{\partial\delta u}{\partial X} + \frac{1}{2}\left(\frac{\partial\delta w}{\partial X}\right)^2 + \frac{\partial w}{\partial X}\frac{\partial\delta w}{\partial X}\right] + A_{22}\left[\frac{1}{R}\frac{\partial\delta v}{\partial\theta} + \frac{\delta w}{R} + \frac{1}{R^2}\frac{\partial w}{\partial\theta}\frac{\partial\delta w}{\partial\theta} + \frac{1}{2R^2}\left(\frac{\partial\delta w}{\partial\theta}\right)^2\right] + B_{12}\left[\frac{\partial\delta\varphi_X}{\partial X}\right] + B_{22}\left[\frac{1}{R}\frac{\partial\delta\varphi_\theta}{\partial\theta}\right] - \delta N_\theta^T\\
\delta N_{X\theta} &= A_{66}\left[\frac{1}{R}\frac{\partial\delta u}{\partial\theta} + \frac{\partial\delta v}{\partial X} + \frac{1}{R}\frac{\partial\delta w}{\partial X}\frac{\partial w}{\partial\theta} + \frac{1}{R}\frac{\partial w}{\partial X}\frac{\partial\delta w}{\partial\theta} + \frac{1}{R}\frac{\partial\delta w}{\partial X}\frac{\partial\delta w}{\partial\theta}\right] + B_{66}\left[\frac{\partial\delta\varphi_\theta}{\partial X} + \frac{1}{R}\frac{\partial\delta\varphi_X}{\partial\theta}\right]\\
\delta Q_\theta &= F_{44}\left[\delta\varphi_\theta(X,\theta) + \frac{1}{R}\frac{\partial\delta w}{\partial\theta}\right]\\
\delta Q_X &= F_{55}\left[\delta\varphi_X(X,\theta) + \frac{\partial\delta w}{\partial X}\right]
\end{aligned} \tag{18}$$

$$\delta M_X = B_{11}\left[\frac{\partial\delta u}{\partial X} + \frac{1}{2}\left(\frac{\partial\delta w}{\partial X}\right)^2 + \frac{\partial w}{\partial X}\frac{\partial\delta w}{\partial X}\right] + B_{12}\left[\frac{1}{R}\frac{\partial\delta v}{\partial\theta} + \frac{\delta w}{R} + \frac{1}{R^2}\frac{\partial w}{\partial\theta}\frac{\partial\delta w}{\partial\theta} + \frac{1}{2R^2}\left(\frac{\partial\delta w}{\partial\theta}\right)^2\right] + D_{11}\left[\frac{\partial\delta\varphi_x}{\partial x}\right] + D_{12}\left[\frac{1}{R}\frac{\partial\delta\varphi_\theta}{\partial\theta}\right] - \delta M_x^T \tag{19}$$

$$\delta M_\theta = B_{12}\left[\frac{\partial \delta u}{\partial X}+\frac{1}{2}\left(\frac{\partial \delta w}{\partial X}\right)^2+\frac{\partial w}{\partial X}\frac{\partial \delta w}{\partial X}\right] + B_{22}\left[\frac{1}{R}\frac{\partial \delta v}{\partial \theta}+\frac{\delta w}{R} + \frac{1}{R^2}\frac{\partial w}{\partial \theta}\frac{\partial \delta w}{\partial \theta} + \frac{1}{2R^2}\left(\frac{\partial \delta w}{\partial \theta}\right)^2\right] + D_{12}\left[\frac{\partial \delta \varphi_X}{\partial X}\right] + D_{22}\left[\frac{1}{R}\frac{\partial \delta \varphi_\theta}{\partial \theta}\right] - \delta M_\theta^T$$

$$\delta M_{X\theta} = B_{66}\left[\frac{1}{R}\frac{\partial \delta u}{\partial \theta}+\frac{\partial \delta v}{\partial X}+\frac{1}{R}\frac{\partial \delta w}{\partial X}\frac{\partial w}{\partial \theta} + \frac{1}{R}\frac{\partial w}{\partial X}\frac{\partial \delta w}{\partial \theta} + \frac{1}{R}\frac{\partial \delta w}{\partial X}\frac{\partial \delta w}{\partial \theta}\right] + D_{66}\left[\frac{\partial \delta \varphi_\theta}{\partial X}+\frac{1}{R}\frac{\partial \delta \varphi_X}{\partial \theta}\right]$$

where A_{ij}, B_{ij}, D_{ij} and F_{ij} are the extensional, coupling, bending, and shear stiffness, respectively and are derived by [16]:

$$\left(A_{ij}, B_{ij}, D_{ij}\right) = \int_{-h/2}^{h/2} Q_{ij}\,(1, z, z^2)dz \quad , \quad (i,j=1,\,2,6)$$
$$(F_{44}, F_{55}) = \int_{-h/2}^{h/2} \frac{K_S E}{2(1+\vartheta)}dz$$
$$Q_{11} = Q_{22} = \frac{E}{1-\vartheta^2}$$
$$Q_{12} = Q_{21} = \frac{\vartheta E}{1-\vartheta^2}$$
$$Q_{66} = \frac{E}{2(1+\vartheta)} \tag{20}$$

where the shear correction factor $K_S = 5/6$ is considered [25]. According to the principle of minimum potential energy, the force equilibrium equations in incremental form can be obtained as follows:

$$\frac{\partial \delta N_X}{\partial X}+\frac{1}{R}\frac{\partial \delta N_{X\theta}}{\partial \theta} = 0$$
$$\frac{\partial \delta N_{X\theta}}{\partial X}+\frac{1}{R}\frac{\partial \delta N_\theta}{\partial \theta} = 0 \tag{21}$$
$$\frac{\partial \delta Q_X}{\partial X}+\frac{1}{R}\frac{\partial \delta Q_\theta}{\partial \theta}+\frac{\partial^2 \delta W}{\partial X^2}(N_X+\delta N_X) + \frac{\partial^2 W}{\partial X^2}\delta N_X - \frac{\partial^2 \delta W}{\partial X^2}\delta N_x^T - \frac{\partial^2 W}{\partial X^2}\delta N_x^T + \frac{2}{R}\frac{\partial^2 \delta W}{\partial X\,\partial \theta}(N_{X\theta}+\delta N_{X\theta}) + \frac{2}{R}\frac{\partial^2 W}{\partial X\,\partial \theta}\delta N_{X\theta} + \frac{1}{R^2}\frac{\partial^2 \delta W}{\partial \theta^2}(N_\theta+\delta N_\theta) + \frac{1}{R^2}\frac{\partial^2 W}{\partial \theta^2}\delta N_\theta - \frac{1}{R^2}\frac{\partial^2 \delta W}{\partial \theta^2}\delta N_x^T - \frac{1}{R^2}\frac{\partial^2 W}{\partial \theta^2}\delta N_x^T - \frac{1}{R}\delta N_x^T - \frac{1}{R}\delta N_\theta = 0$$
$$\frac{\partial \delta M_X}{\partial X}+\frac{1}{R}\frac{\partial \delta M_{X\theta}}{\partial \theta} - \delta Q_X = 0$$
$$\frac{\partial \delta M_{X\theta}}{\partial X}+\frac{1}{R}\frac{\partial \delta M_\theta}{\partial \theta} - \delta Q_\theta = 0$$

Substituting resultant forces and moments derived in Eqs. (18), (19) into Eq. (21) leads to a set of nonlinear displacement equilibrium equations in the incremental form. For instance, the first equation of (21) is described in detail:

$$\begin{aligned}
&A_{11}\left[\frac{\partial^2\delta u}{\partial X^2}+\frac{\partial^2\delta w}{\partial X^2}\frac{\partial\delta w}{\partial X}+\frac{\partial^2 w}{\partial X^2}\frac{\partial\delta w}{\partial X}\right.\\
&\quad\left.+\frac{\partial^2\delta w}{\partial X^2}\frac{\partial w}{\partial X}\right]\\
&\quad+A_{12}\left[\frac{1}{R}\frac{\partial^2\delta v}{\partial X\partial\theta}\frac{1}{R}\frac{\partial w}{\partial X}\right.\\
&\quad+\frac{1}{R^2}\frac{\partial^2\delta w}{\partial X\partial\theta}\frac{\partial\delta w}{\partial\theta}\\
&\quad+\frac{1}{R^2}\frac{\partial^2\delta w}{\partial X\partial\theta}\frac{\partial w}{\partial\theta}\\
&\quad\left.+\frac{1}{R^2}\frac{\partial^2 w}{\partial X\partial\theta}\frac{\partial\delta w}{\partial\theta}\right]\\
&\quad+B_{11}\left[\frac{\partial^2\delta\varphi_X}{\partial X^2}\right]\\
&\quad+B_{12}\left[\frac{1}{R}\frac{\partial^2\delta\varphi_\theta}{\partial X\partial\theta}\right]\\
&\quad+\frac{1}{R}A_{66}\left[\frac{1}{R}\frac{\partial^2\delta u}{\partial\theta^2}+\frac{\partial^2\delta v}{\partial X\partial\theta}\right.\\
&\quad+\frac{1}{R}\frac{\partial^2 w}{\partial X\partial\theta}\frac{\partial\delta w}{\partial\theta}\\
&\quad+\frac{1}{R}\frac{\partial^2\delta w}{\partial X\partial\theta}\frac{\partial\delta w}{\partial\theta}\\
&\quad+\frac{1}{R}\frac{\partial\delta w}{\partial X}\frac{\partial^2 w}{\partial\theta^2}\\
&\quad+\frac{1}{R}\frac{\partial w}{\partial X}\frac{\partial^2\delta w}{\partial\theta^2}\\
&\quad\left.+\frac{1}{R}\frac{\partial\delta w}{\partial X}\frac{\partial^2\delta w}{\partial\theta^2}\right]\\
&\quad+\frac{1}{R}B_{66}\left[\frac{\partial^2\delta\varphi_\theta}{\partial X\partial\theta}\right.\\
&\quad\left.+\frac{1}{R}\frac{\partial^2\delta\varphi_X}{\partial\theta^2}\right]=0
\end{aligned}\tag{22}$$

The FG cylinder is considered just subjected to a thermal gradient along the thickness direction. The clamped and simply supported boundary conditions in terms of constraints on displacements, stress resultants, and stress couples at $x=0,L$, are as follows:

Clamped—in-plane movable:

$$N_X = v = w = \varphi_X = \varphi_\theta = 0 \tag{23}$$

Simply supported—in-plane movable:

$$N_X = M_X = v = w = \varphi_\theta = 0 \tag{24}$$

And in Clamped condition at $y=0.b \quad y\to(R\theta)$:

$$u = v = w = \varphi_X = \varphi_\theta = 0 \tag{25}$$

Numerical solution

In this paper, the DR method combined with a finite difference discretization method is used. The DR is an efficient technique and an explicit iterative method which is applied to transfer a boundary value problem into a time-stepping initial value problem. In this case, artificial inertia and damping forces are added to the right side of Eq. (21) as follows [16]:

$$LHS\{Eqs.\ (21)\} = m_X\frac{\partial^2\delta X}{\partial t^2}+c_X\frac{\partial\delta X}{\partial t}$$

In Eq. (26) LHS = left-hand side and m_X, c_X $(X=u,v,w,\varphi_X,\varphi_\theta)$ are elements of diagonal fictitious mass and damping matrices m and c, respectively. To check the numerical accuracy, the element of diagonal mass matrix m is derived by the Gershgörin theorem as [27, 28]:

$$m_{ii}{}^X \geq 0.25(\tau^n)^2\sum_{j=1}^{N}\left|k_{ij}{}^X\right|$$

where superscript n mentions the nth iteration and τ is the increment of fictitious time which its value is assumed to 1. Moreover, k_{ij} is the element of stiffness matrix K which is obtained by:

$$K=\frac{\partial P}{\partial X} \tag{28}$$

where P is the left-hand-side of the equilibrium relation (21). Also, by applying the Rayleigh principle to each node, the instant critical damping factor c_i^n for node i at the n^{th} iteration is achieved as [29]:

$$c_i^n = 2\left\{\frac{(X_i^n)^T(P_i^n)}{(X_i^n)^T m_{ii}^n X_i^n}\right\}^{\frac{1}{2}} \tag{29}$$

Besides, to make the elements of diagonal fictitious damping matrix C , various C values for diverse nodes are obtained at each direction as [29]:

$$c_{ii} = c_j m_{ii},\quad i,j=1,2,\dots,N \tag{30}$$

Eventually, the velocity and acceleration terms should be replaced with the equivalent central finite-difference terms as follows:

$$\ddot{X}^n = \frac{\dot{X}^{n+\frac{1}{2}}-\dot{X}^{n-\frac{1}{2}}}{\tau^n} \tag{31}$$

$$\dot{X}^{n-\frac{1}{2}} = \frac{X^n - X^{n-1}}{\tau^n} \tag{32}$$

By substituting Eqs. (31) and (32) into the right-hand side of Eq. (26), the stability equations can be written into an initial value form as:

$$\delta\dot{u}_i^{\,n+1/2} = \frac{2\tau^n}{2+\tau^n c_i^n}(m_{ii}^n)^{-1}\left(\frac{\partial \delta N_X}{\partial X} + \frac{1}{R}\frac{\partial \delta N_{X\theta}}{\partial \theta}\right)_i^n + \frac{2-\tau^n c_i^n}{2+\tau^n c_i^n}\delta\dot{u}_i^{\,n-1/2}$$
$$\delta\dot{v}_i^{\,n+1/2} = \frac{2\tau^n}{2+\tau^n c_i^n}(m_{ii}^n)^{-1}\left(\frac{\partial \delta N_{X\theta}}{\partial X} + \frac{1}{R}\frac{\partial \delta N_{\theta}}{\partial \theta}\right)_i^n + \frac{2-\tau^n c_i^n}{2+\tau^n c_i^n}\delta\dot{v}_i^{\,n-1/2}$$
$$\delta\dot{w}_i^{\,n+1/2} = \frac{2\tau^n}{2+\tau^n c_i^n}(m_{ii}^n)^{-1}\left(\frac{\partial \delta Q_X}{\partial X} + \frac{1}{R}\frac{\partial \delta Q_{\theta}}{\partial \theta} + \frac{\partial^2 \delta W}{\partial X^2}(N_X+\delta N_X) + \frac{\partial^2 W}{\partial X^2}\delta N_X + \frac{2}{R}\frac{\partial^2 \delta W}{\partial X\,\partial\theta}(N_{X\theta}+\delta N_{X\theta}) + \frac{2}{R}\frac{\partial^2 W}{\partial X\,\partial\theta}\delta N_{X\theta} + \frac{1}{R^2}\frac{\partial^2 \delta W}{\partial \theta^2}(N_\theta+\delta N_\theta) + \frac{1}{R^2}\frac{\partial^2 W}{\partial \theta^2}\delta N_\theta - \frac{1}{R}\delta N_\theta\right)_i^n + \frac{2-\tau^n c_i^n}{2+\tau^n c_i^n}\delta\dot{w}_i^{\,n-1/2} \tag{33}$$
$$\delta\dot{\varphi}_{Xi}^{\,n+1/2} = \frac{2\tau^n}{2+\tau^n c_i^n}(m_{ii}^n)^{-1}\left(\frac{\partial \delta M_X}{\partial X} + \frac{1}{R}\frac{\partial \delta M_{X\theta}}{\partial \theta} - \delta Q_X\right)_i^n + \frac{2-\tau^n c_i^n}{2+\tau^n c_i^n}\delta\dot{\varphi}_{Xi}^{\,n-1/2}$$
$$\delta\dot{\varphi}_{\theta i}^{\,n+1/2} = \frac{2\tau^n}{2+\tau^n c_i^n}(m_{ii}^n)^{-1}\left(\frac{\partial \delta M_{X\theta}}{\partial X} + \frac{1}{R}\frac{\partial \delta M_{\theta}}{\partial \theta} - \delta Q_\theta\right)_i^n + \frac{2-\tau^n c_i^n}{2+\tau^n c_i^n}\delta\dot{\varphi}_{\theta i}^{\,n-1/2}$$

By integrating the velocities at the end of each load step, the incremental displacements can be achieved by:

$$\delta X^{n+1} = \delta X^n + \Delta\tau^{n+1}\delta\dot{X}^{n+\frac{1}{2}} \tag{34}$$

To compute the critical thermal buckling load from the load-displacement curve, the total displacements of each load must be obtained. Hence, the computed incremental displacements in each load step should be added to the displacements (determined from the previous load steps) as follows:

$$X^n = X^{n-1} + \delta X^n \tag{35}$$

It is obvious that the critical thermal buckling load is a specified load in which a large amount of displacement is occurred compared to the previous load steps.

Fig. 2 represents the convergence behavior of the DR method of the critical buckling temperature difference versus Q. Here, Q is an equivalence point which shows the number of nodes in longitudinal direction (*M=20*), and the number of nodes in circumferential direction (*N=10*). As seen, from the point 20*10, the results converged. It is also noted that 15 nodes are considered along the thickness direction.

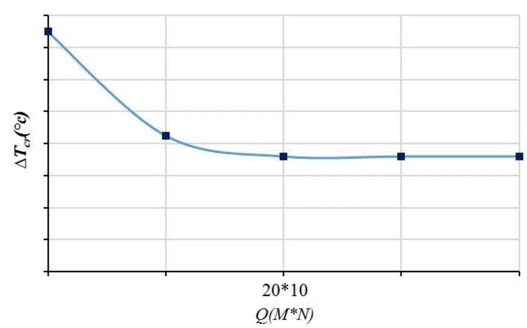

Fig 2. The convergence behavior of the DR technique of the critical buckling temperature difference versus Q (an equivalence point).

For better clarification of the procedure for the buckling investigation, it can be noted that the thermal load is applied to the plate incrementally so that, in each load step, the incremental form of the governing mathematical relations can be solved by a numerical code prepared via the DR technique. After usingthe DR code in the first increment, the latter load step is added to the previous one, and the program is repeated again. Moreover, it should be mentioned that at the end of the convergence in each load step, the obtained displacement is also added to those computed in the previous one. This process continues till the code diverges, and this is a sign of buckling event. Briefly, when the buckling occurs, a huge amount of displacement will be observed in the thermal load-displacement curve at a certain load. In Fig. 3, the temperature difference diagram versus the displacement for a cylindrical panel with 90° panel angle with clamped-clamped boundary condition is shown, for obtaining the thermal buckling load. As can be seen, by an incremental increase in the temperature, a significant deflection has occurred in temperature above 1200°C.

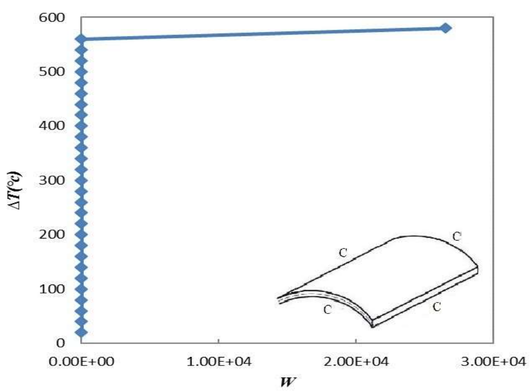

Fig 3. Temperature difference versus displacement for cylindrical panel with clamped – clamped boundary condition

Due to the very long terms of governing equations in the displacement field, as an example, Eq. (33) has been written based on force stability equation (Eq. (21)). Here, however, the developed numerical code is based on displacement relations. Therefore, the displacement stability equations and Eqs. (33) to (35) with the relevant boundary conditions in their finite-difference forms, constitute the set of equations for the sequential DR approach. The DR algorithm is explained in [30, 31] in details.

Results and discussions

In this paper, nonlinear thermal buckling of moderately thick FG cylindrical panels made of combinations of aluminum and alumina has been studied. The properties such as modulus of elasticity, thermal conductivity, and thermal expansion coefficients and the Poisson's ratio of metal and ceramic phases are: $E_m = 70\ GPa$, $K_m = 204\ W/mK$, $\propto_m = 23 \times 10^{-6}\ (1/°C)$, $\vartheta_m = 0.3$ $E_c = 380\ GPa$, $K_c = 10.4W/mK$, $\propto_c = 7.4 \times 10^{-6}\ (1/°C)$, $\vartheta_c = 0.22$, respectively. Furthermore, the thickness of panels are assumed as $h = 0.001m$. Although the temperature of the metal phase is considered constant at T_m =20 C, the temperature of the ceramic phase rises incrementally. In fact, the nonlinear and linear temperature distributions are considered along the thickness direction. The final purpose is to find the critical temperature difference $\Delta T_{cr} = (T_c - T_m)$ which causes the thermal buckling.

Tables 1 and 2 compare DR results of the present study with those reported by Ref. [24] for simply supported FG cylindrical shell subjected to the linear distribution of thermal loads. Moreover, the values in Table 1 are given for a certain radius ($R = 0.5\ m$) with different length-to-radius ratios and various thickness-to-radius ratios. Also, the values in Table 2 are given for different sizes of radius $R(m)$ and thickness $h(m)$ with the certain length-to-radius ratio ($L\ /\ R = 0.5$). In these cases, the Poisson's ratio is considered as $\vartheta = 0.3$. As indicated in Tables 1 and 2, there is a good agreement between the current results and those reported by Ref. [24] for thermal buckling of FG cylindrical shells subjected to linear temperature distribution with different geometries, grading indices, and boundary conditions.

Table 1: Comparison of the critical temperature difference (°C) for the simply supported FG cylindrical shell ($k = 1, R = 0.5m$) based on linear temperature distribution achieved by the DR technique and the results reported by Ref. [24].

h/R	L/R					
	0.15		0.3		0.5	
	Ref. [24]	Present study	Ref. [24]	Present study	Ref. [24]	Present study
0.0046	140	140	100	80	40	40
0.0064	200	210	120	120	80	60
0.00822	320	320	180	180	80	80
0.001	400	420	240	240	100	100

Table 2: Comparison of the critical temperature difference (℃) of the simply supported FG cylindrical shell ($k = 1, L/R$=0.5) based on linear temperature distribution obtained by the DR method and the results obtained by Ref. [24].

$R(m)$	$h(m)$					
	0.005		0.007		0.01	
	Ref. [24]	Present study	Ref. [24]	Present study	Ref. [24]	Present study
0.625	100	80	300	300	1000	1000
0.90	60	55	180	170	500	520
1.18	60	80	120	120	340	330
1.45	60	60	100	90	260	230
1.73	60	60	80	70	220	180
2.00	60	60	60	60	160	160

In Fig. 4, the critical temperature difference is illustrated in terms of the grading index in the simple power-law model for the radius-to-thickness ratio of 5 and the length-to-radius of 0.5 for two types of heat distribution (linear and nonlinear) and 180° angle with simply supported-clamped and clamped-clamped boundary conditions. As seen, based on linear thermal load distribution the highest difference of critical thermal load, between two cases of clamped and simply supported boundary conditions, is occurred in grading index of zero (ceramic phase) and by the increase of grading index, the difference of thermal buckling decreases between clamped and simply supported boundary conditions. However, based on nonlinear thermal load distribution, there is not any significant difference between clamped and the simply supported boundary conditions for various grading indices.

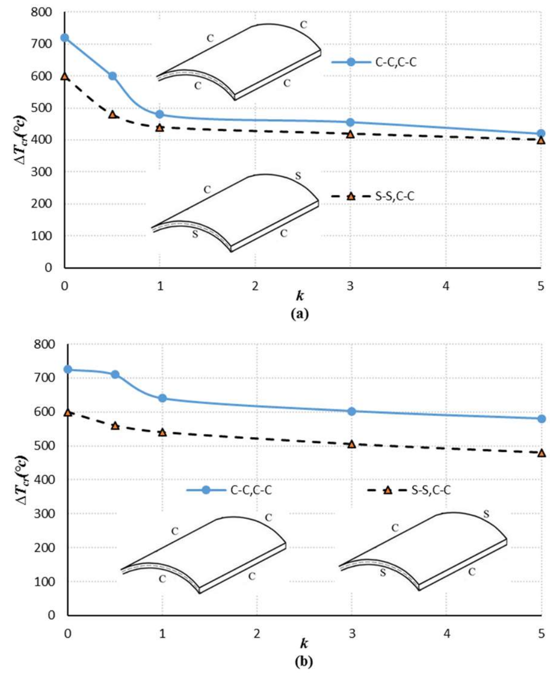

Fig 4. Critical temperature differences (℃) versus the grading index based on the simple power-law model for various boundary conditions (a) Linear thermal load distribution (b) Nonlinear thermal load distribution.

Fig. 5 illustrates the effects of changes of the grading indices in the Mori-Tanaka model on critical temperature difference with different boundary conditions for linear and nonlinear analysis with 180-degree panel angle and radius-to-thickness ratio of 5 ($R/h = 5$) and length-to-radius ratio of 0.5 ($L/R = 0.5$). The Poisson coefficient is assumed to be constant for the simple power-law model, but in the Mori-Tanaka model, the Poisson coefficient changes along the thickness considering the equations (2-5). By comparing the results between these two types of Models (Fig. 4 and Fig. 5) considered for the cylindrical panel, it can be seen that the critical temperature difference based on the Mori-Tanaka model is greater than the power-law one for different boundary conditions. In other words, the Mori-Tanaka model has higher temperature endurance and higher buckling temperature than the simple power-law model.

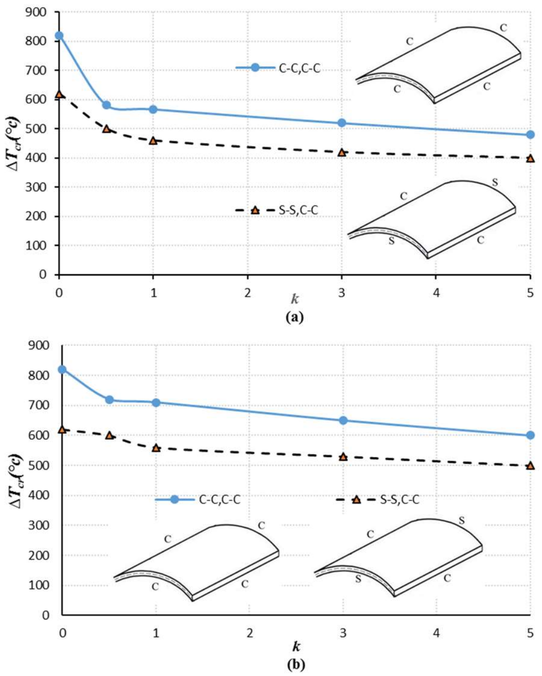

Fig 5. Critical temperature differences (℃) versus the grading index based on the Mori-Tanaka model with different boundary conditions (a) Linear thermal distribution (b) Nonlinear thermal load distribution

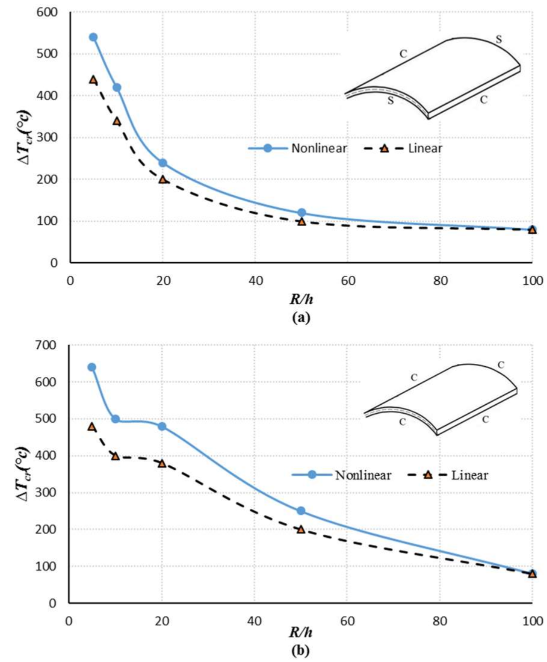

Fig 6. The values of critical temperature difference (℃) versus the ratio of radius-to-thickness ratio for various thermal load distributions (A). Simply supported - Clamped (S-S, C-C) (B) Clamped-Clamped (C-C, C-C)

Fig. 6 shows the critical temperature difference of different radius to thickness ratios for grading index $k = 1$ and the ratio of the length to radius ratio of 0.5 ($L/R = 0.5$) with two types of thermal load distribution (linear and nonlinear) for 180 degree of panel angle as well as different boundary conditions. It can be seen, with the increase of radius to thickness ratio, the critical temperature difference of buckling decreases. Also, by decreasing radius-to-thickness ratio, the difference between two cases of linear and nonlinear thermal load distributions' results increases.

Fig. 7 illustrates the critical temperature difference for different ratios of length-to-radius ratios, considering the ratio of radius to thickness 5 and the grading index of 0.5 and the panel angel of 180° for simply supported-clamped and clamped-clamped boundary conditions. As indicated, the effect of the length-to-radius ratio on the thermal buckling load is considerable for the ratios smaller than 1 and 2 for simply supported and clamped boundary conditions, respectively. Also, by increasing the length-to-radius ratio from 2, the thermal buckling load remains approximately constant.

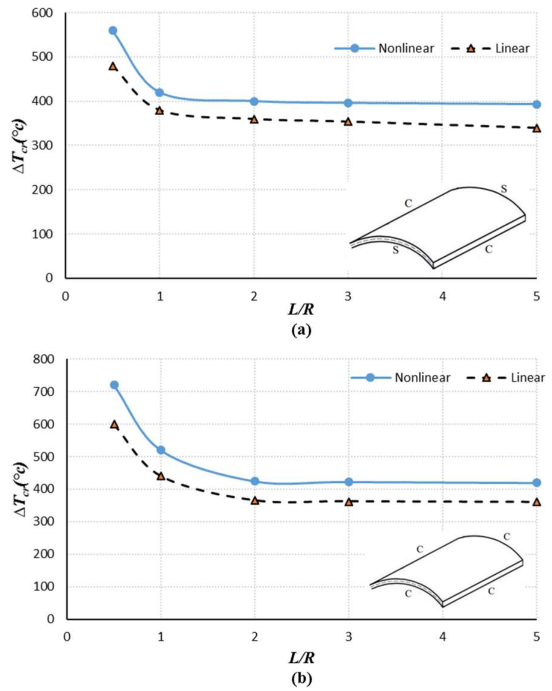

Fig 7. Critical temperature difference values (℃), in terms of length to radius ratio, for different thermal distributions (A) (S-S, C-C) (B) (C-C, C-C)

To study the effect of panel angles on the critical buckling temperature difference, the buckling temperature difference graph for various grading indices with radius- to-thickness ratio of 10 and length-to-radius ratio of 0.5 at various boundary conditions are shown in Fig. 8 for linear and nonlinear thermal loads distribution. It can be seen that by increasing the panel angle, the difference in critical buckling temperature in various boundary conditions decreases. Also, by comparing the critical temperature difference in cylindrical panels with 90° angle with other angles, it is observed that in the 90° angle, the structure endures a higher temperature than the other angles. Moreover, in the grading index of zero (ceramic), there is no difference between the distribution of linear and nonlinear thermal load on the critical temperature difference for a cylindrical panel with 90° angle in different boundary conditions. By increasing θ from 90 ° to 180 °, there is a significant decrease in the critical temperature difference, and in this range, θ has the greatest impact on metallic phase ($k = 0$). In simply supported boundary conditions with increasing k from 0 to 5, there is no significant difference between the results but in clamped boundary condition the mentioned difference is slightly higher. Moreover, in the case of nonlinear thermal load distribution, the difference between the diagrams for different indices is much greater than the linear thermal distribution.

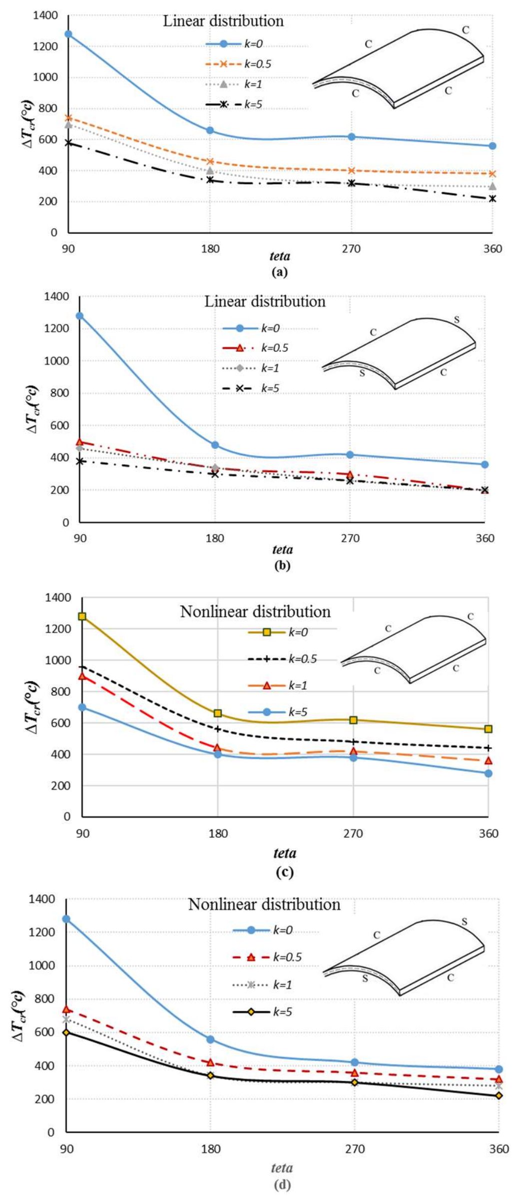

Fig 8. Critical temperature difference values (℃) in different angles for various grading indices of: (a) linear thermal load distribution, clamped-clamped boundary condition, (b) linear thermal load distribution, simply supported-clamped boundary condition, (c) nonlinear thermal load distribution,

clamped-clamped boundary condition (d) nonlinear thermal distribution, simply supported-clamped boundary condition.

Conclusion

In the present paper, thermal buckling of FG cylindrical panels has been considered with clamped and simply supported boundary conditions using FSDT and large deflection von Kármán equations. The properties of the constituent components of the FG panel are considered to change continuously and smoothly along the thickness direction based on simple power-law and Mori–Tanaka distributions. The results are obtained for both linear and nonlinear temperature distributions. The critical buckling load is predicted based on the thermal load-displacement curve obtained by solving the incremental form of nonlinear equilibrium equations. The DR technique combined with the central finite difference discretization method is utilized for solving the incremental equations. Eventually, the influences of boundary conditions, rules of mixture, grading indices, radius -to- thickness, and length-to-radius ratios are studied on thermal buckling loads. The significant results are as follows:

Based on nonlinear thermal load distribution, there is not any significant difference between the results of clamped and the simply supported boundary conditions for various grading indices.

It is observed that the grading index has a significant impact on the thermal buckling of FG panels.

The length-to-radius ratio has a considerable effect on the thermal buckling load for the smaller ratios (almost less than 1) in different boundary conditions.

By decreasing the radius-to-thickness ratio, differences between the thermal buckling load obtained by linear and nonlinear thermal load distributions increase.

The Mori-Tanaka model predicts greater thermal buckling load than the simple rule of mixture.

The effect of the length-to-radius ratio on the thermal buckling load is considerable for the ratios smaller than 2 and by increasing the ratio from 2, the thermal buckling load remains approximately constant.

References

[1] Z. X. Lei, L. W. Zhang, K. M. Liew, Analysis of laminated CNT reinforced functionally graded plates using the element-free kp-Ritz method, COMPOS PART B-ENG, 84 (2016) 211-221.

[2] L. W. Zhang, Z. G. Song, K. M. Liew, Computation of aerothermoelastic properties and active flutter control of CNT reinforced functionally graded composite panels in supersonic airflow, Comput. Methods Appl. Mech. Engrg., 300 (2016) 427-441.

[3] Z. X. Lei, L. W. Zhang, K. M. Liew, Elastodynamic analysis of carbon nanotube-reinforced functionally graded plates, Int. J. Mech. Sci., 99 (2015) 208-217.

[4] L. W. Zhang, K. M. Liew, geometrically nonlinear large deformation analysis of functionally graded carbon nanotube reinforced composite straight-sided quadrilateral plates, Comput. Methods Appl. Mech. Engrg., 295 (2015) 219-239.

[5] L. W. Zhang, Z. G. Song, K. M. Liew, Nonlinear bending analysis of FG-CNT reinforced composite thick plates resting on Pasternak foundations using the element-free IMLS-Ritz method, Compos. Struct., 128 (2015) 165-175.

[6] L. W. Zhang, K. M. Liew, Large deflection analysis of FG-CNT reinforced composite skew plates resting on Pasternak foundations using an element-free approach, Compos. Struct., 132 (2015) 974-983.

[7] P. Zhu, L. W. Zhang, K. M. Liew, Geometrically nonlinear thermomechanical analysis of moderately thick functionally graded plates using a local Petrov-Galerkin approach with moving Kriging interpolation, Compos. Struct., 107 (2014) 298-314.

[8] L. W. Zhang, K. M. Liew, J. N. Reddy, Postbuckling behavior of bi-axially compressed arbitrarily straight-sided quadrilateral functionally graded material plates, Comput. Methods Appl. Mech. Engrg., 300 (2016) 593-610.

[9] H. Shen Shen, Y. Xiangc, J.N. Reddy, Thermal postbuckling behavior of FG-GRC laminated cylindrical panels with temperature-dependent properties, Compos Struct, 211(2019) 433-442.

[10] J. Morais, F. Silva, Influence of modal coupling and geometrical imperfections on the nonlinear buckling of cylindrical panels under static axial load, ENG STRUCT, 183 (2019) 816–829.

[11] N. Silvestre, A. Duartea, J. Martins, S. Silvab, GBT Buckling Analysis of Cylindrical Panels Under Compression, Struct. 17 (2019) 34-42.

[12] H. Norouzi, A. Alibeigloo, Three dimensional thermos viscoelastic analysis of a simply supported FGM cylindrical panel, Compos Struct 148 (2016) 181–190.

[13] R. Seifi, H. Saeidi Googarchin, M. Farrokhi, Buckling of cracked cylindrical panels under axially compressive and tensile loads, TWS, 94 (2015)457–465.

[14] D. Panahandeh-Shahraki, A. Shahidi, H. Mirdamadi, O. Vaseghi, Nonlinear analysis of uni-lateral buckling for

cylindrical panels on tensionless foundation, TWS, 62 (2013) 109–117.
[15] K. Magnucki, Elastic buckling of a cylindrical panel with symmetrically varying mechanical properties – analytical study, Compos Struct 204 (2018) 217-222.
[16] M. E. Golmakani, M. N. Sadraee Far, M. Moravej, Dynamic relaxation method for nonlinear buckling analysis of moderately thick FG cylindrical panels with various boundary conditions, JMST 30 (2016) 5565–5575.
[17] L. W. Zhang, P. Zhu, K. M. Liew, Thermal buckling of functionally graded plates using a local Kriging meshless method, Compos. Struct., 108 (2014) 472-492.
[18] N. D. Duc, H. V. Tung, Nonlinear response of pressure loaded functionally graded cylindrical panels with temperature effects, Compos. Struct., 92 (2010) 1664-1672.
[19] K. M. Liew, X. Zhao, Y. Y. Lee, Postbuckling responses of functionally graded cylindrical shells under axial compression and thermal loads, Compos Part B, 43 (2012) 1621-1630.
[20] X. Zhao, K. M. Liew, A mesh-free method for analysis of the thermal and mechanical buckling of functionally graded cylindrical shell panels, Comput. Mech, 45 (2010) 297-310.
[21] X. Zhao, K. M. Liew, An element-free analysis of mechanical and thermal buckling of functionally graded conical shell panels, Int. J. Numer. Methods Eng., 86 (2011) 269-285.
[22] D. V. Dung, L. K. Hoa, Nonlinear analysis of buckling and postbuckling for axially compressed functionally graded cylindrical panels with the poisson's ratio varying smoothly along the thickness, Vietnam J. Mech., 34 (2012) 27-44.
[23] ND. Duc, PT. Thang, Nonlinear response of imperfect eccentrically stiffened ceramic-metalceramic FGM thin circular cylindrical shells surrounded on elastic foundations and subjected to axial compression. Comp Struct;110 (2014) 200–206.
[24] R .Shahsiah, MR. Eslami, Thermal buckling of functionally graded cylindrical shell, J Therm Stresses, 26 (2003) 277–294.
[25] JN. Reddy, Mechanics of Laminated Composite Plates and Shells, Second Edition, CRC Press, New York; 2004.
[26] ND. Duc, PT. Thang, Nonlinear response of imperfect eccentrically stiffened ceramic-metalceramic FGM thin circular cylindrical shells surrounded on elastic foundations and subjected to axial compression. Comp Struct 110 (2014) 200–206.
[27] P. Underwood, Dynamic relaxation, in computational methods for transient analysis, Chapter 5. Amsterdam, Elsevier; 1983.
[28] LC. Zhang, TX. Yu, Modified adaptive dynamic relaxation method and application to elastic–plastic bending and wrinkling of circular plate. Comput Struct, 33 (1989) 609–14.
[29] LC. Zhang, M. Kadkhodayan, Y-W. Mai, Development of the maDR method. Comput Struct 52 (1994),1–8.
[30] ME. Golmakani, M. Kadkhodayan, Nonlinear bending analysis of annular FGM plates using higher-order shear deformation plate theories. Compos Struct, 93 (2011) 973–982.
[31] ME. Golmakani, M. Kadkhodayan, Large deflection analysis of circular and annular FGM plates under thermo-mechanical loadings with temperature-dependent properties. Compos Part B, 42 (2011) 614–25.

JAST, Vol. 14, No. 2, pp. 66-79
© Iranian Aerospace Society, Summer-Fall 2021

Received: 12 October 2020
Accepted: 27 April 2021